HEAT TRANSFER
https://onlinelibrary.wiley.com/journal/26884542
Online ISSN:2688-4542
Accepted - December 2nd 2022.

Analysis of dissipative non-Newtonian magnetic polymer flow from a curved stretching surface with slip and radiative effects

M. Gnaneswara Reddy[1], D. Tripathi[2]* and O. Anwar Bég[3]

[1]Department of Mathematics, Acharya Nagarjuna University Campus, Ongole - 523 001, Andhra Pradesh, India, mgrmaths@gmail.com

[2]Department of Mathematics, National Institute of Technology, Uttarakhand-246174, India. E-mail: dtripathi@nituk.ac.in

*[3]Multi-Physical Engineering Sciences Group, Dept. Mechanical and Aeronautical Engineering, Corrosion/Coatings Lab, 3-08, SEE Building, Salford University, Manchester, M54WT, **UK**. O.A.Beg@salford.ac.uk*

Abstract

The convective-radiative magnetohydrodynamic non-Newtonian second grade fluid boundary layer flow from a curved stretching surface has been scrutinized in the present study. The Reiner-Rivlin second grade viscoelastic model is deployed which provides a good approximation for certain magnetic polymers. High temperature invokes the presence of radiative heat transfer which is simulated with the Rosseland diffusion approximation. Viscous dissipation and Joule heating are also featured in the model and hydrodynamic (velocity) slip at the wall is also incorporated in the boundary conditions. The emerging nonlinear coupled dimensionless transport equations are solved with a Runge-Kutta method and a shooting numerical scheme. The influence of emerging multi-physical flow parameters on the dimensionless profiles are examined with the help of plots for comparative analysis of both non-Newtonian fluid and Newtonian fluid. The numerical solutions are validated for special cases with existing works. The velocity declines for higher magnetic field whereas the reverse trend is noted for the temperature function. An augmentation in thermal field is noted with increment in radiation parameter. Furthermore, the fluid temperature of second grade fluid is higher with increasing Brinkmann number. Wall slip induces deceleration. Contour plots for streamlines and isotherms are also visualized and analyzed.

Keywords: *Joule heating, MHD, thermal radiation, second grade fluid, curved surface, velocity slip, electroconductive polymer processing.*

1. Introduction

Transport from curved surfaces is an important topic in numerous industrial systems including manufacturing, coating, materials processing and also aerodynamics of flight vehicles. The compressible flow from a curved surface was initially investigated by Kaplan [1]. Later, motivated by industrial coating systems, the incompressible flow of a Newtonian liquid from a linear stretching surface was analysed by Crane [2] in the year 1970. More recently viscous fluid flow over a curved stretching sheet was examined by Sajid *et al.* [3] who deployed a similarity approach for reducing the governing boundary flow equations and observed that the momentum boundary layer thickness was reduced with higher curvature. Abbas *et al.* [4] have reported the flow and heat transfer flow along a curved surface in the presence of applied magnetic field. Further studies of boundary layer flows from curved stretching surfaces have considered a diverse spectrum of multi-physical phenomena including non-Fourier and non-Darcy effects [5], unsteady and wall suction/injection effects [6], exponential wall stretching [7], power-law wall stretching [8], chemical reactions [9], nanofluids [10], entropy generation [11], radiative heat transfer [12], convective wall boundary conditions [13], porous media drag [14], wall slip [15], oblique stagnation flow [16], thermal conductivity variation [17] and activation energy and mass diffusion [18]. All these studies indicated that curvature plays a prominent role in modifying the boundary layer characteristics including Nusselt number and wall shear stress.

Fluid flow in the presence of a magnetic field has prominent applications in metallurgical engineering, electro-conductive polymer processing, nuclear reactor thermal control, plastics manufacture etc. The science of magnetohydrodynamics (MHD) is used to analyse the interaction of external magnetic field on electrically conducting liquids. MHD materials processing is for example very useful in achieving non-intrusive control of fabrication processes. Mathematical modelling of curved stretching sheet deposition flows with MHD effects has therefore mobilized considerable interest in recent years in applied mathematics and engineering sciences. Magnetic effects may include Lorentzian drag, magnetic induction, Ohmic heating, Maxwell displacement currents and also static or time-dependent magnetic fields. The unsteady hydromagnetic boundary layer flow external to a curved stretching surface was analysed by Naveed *et al.* [19]. The Runge-Kutta integrating was employed and benchmarked with the special case of a flat unsteady stretching surface (infinite curvature). The thermal analysis of nanofluid flow from a curved surface was scrutinized by Mishra et al. [20]. The interaction of hydromagnetic flow of a nanofluid from a curved nonlinearly extending

sheet with higher order wall slip and thermo-diffusion effects has been explored by Ibrahim and Kuma [21] who utilized the bvp4c numerical procedure in MATLAB. It noted that the flow is decelerated with first and third order slip parameters but accelerated with second order slip. The local mass transfer rate at the wall (Sherwood number) is enhanced with Soret and Dufour numbers whereas the local heat transfer rate (Nusselt number) is suppressed. The hydromagnetic and viscous liquid flow with thermal radiative flux was scrutinized by Hayat *et al.* [22]. It observed that velocity and skin friction are depleted with stronger applied magnetic field i. e. Hartmann number and heat transfer rate is also reduced with increasing curvature parameter. The thermal radiation impact on convective flow from a stretching cylinder has been addressed by Pandey and Kumar [23]. Pandey and Upreti [24] have analyzed the effect of heat generation on transport from a curved sheet and observed that the rate of heat transfer is reduced for larger curvature. Temperature and thermal boundary layer thickness was also shown to be elevated with Biot number and radiative parameter. Riaz *et al.* [25] studied the entropy generation in magneto-convective radiative nanofluid from a curved extending surface. Bhatti *et al.* [26] have simulated the convective and dissipative flow of a third-grade viscoelastic fluid in microchannel under electrical and magnetic field influence.

In recent years a new generation of intelligent polymers known as electro-conductive or magneto-rheological polymers [27] has emerged. These sophisticated liquids combine magnetohydrodynamics with rheology i.e. non-Newtonian behaviour. Such materials provide enhanced performance in for example coating applications in aerospace, biomedical and marine industries. Electro-conductive polymers may exhibit a range of rheological effects including shear thinning (pseudoplasticity), shear thickening (dilatancy) and viscoelasticity (stress relaxation and retardation). Scientists have therefore considered a range of such models in recent years. Shahid *et al.* [28] used the Maxwell viscoelastic model to study magnetized polymer flow from a stretching surface with non-Fourier heat flux. Micropolar non-Newtonian hydromagnetic flow from a curved extending sheet was explored by Naveed *et al*. [29]. Bisht and B*ég* [30] investigated the non-Newtonian magnetic nanofluid flow doped with micro-organisms from a curved stretching surface using the Sisko high shear rate model. The heat transfer characteristics of power-law rheological nanofluids from a stretching sheet has been examined by Reddy *et al.* [31]. Shabbir *et al.* [32] obtained finite difference numerical solutions for magneto-convective flow of a micropolar fluid from a curved stretching boundary. It showed that the flow is decelerated with stronger magnetic parameter, power law index and radius of curvature whereas micro-rotation is elevated. Maity and Kundu [33] studied the viscoplastic (Casson) nanofluid transport from a curved stretching sheet in the presence of

applied magnetic field, observing that temperature and concentration are reduced with increasing stretching parameter. The magnetohydrodynamic Sutterby non-Newtonian nanoparticle-doped drug delivery with heat transfer in a tapered artery was studied by Bhatti et al. [34].

In high temperature magnetic materials processing, both thermal radiation and Joule heating (Ohmic dissipation) may arise. Other systems featuring these phenomena include thermal energy conversion processes, photochemical magnetic bioreactors and liquid metal fabrication. Zhang *et al.* [35] have computed Joule heating effects on stagnation point flow of magnetic nanofluid from a curved stretching or contracting permeable surface. It is noted that greater curvature reduces surface skin friction whereas larger wall suction induces the opposite effect. It is also observed that wall heat transfer rate is boosted with wall suction, greater Hartmann number and Biot number. Magnetohydrodynamic Newtonian thermo-solutal flow from a curved stretching sheet with thermal radiation and Joule Heating was investigated by Hayat *et al.* [36]. It is noted that pressure, skin friction coefficient, and Nusselt number decrease with larger curvature parameter and that Joule heating strongly modifies the temperature field. Anantha Kumar *et al.* [37] have scrutinized the effect of thermal radiation in viscoplastic convection from a curved stretching surface, employing the Rosseland model and Runge–Kutta methods. They found that the Casson viscoplastic parameter decreases velocities whereas the curvature parameter increases them. Ferdows *at al.* [38] studied the impact of radiative flux on hydromagnetic flow from a curved stretching sheet, using MATLAB bvp4c quadrature, noting that the fluid velocity and temperature increase with curvature parameter whereas higher magnetic parameter reduces velocity. Sridhar *et al*. [39] have reported the combined effects of Joule heating and radiation on non-Newtonian fluid flow. Further analyses reporting on the dual effects of thermal radiation and Ohmic heating on stretching sheet flows include Sajid *et al.* [40] (on ferrofluids), Shamshuddin *et al.* [41, 42] (on micropolar magnetic polymers and pseudoplastic magnetic polymers), and Prakash *et al.* [43] (who used a tangent hyperbolic rheological model for bi-axial electromagnetohydrodynamic stretching flow).

The above studies have not considered the viscoelastic second grade Reiner-Rivlin model which provides a good approximation for certain magnetic rheological polymers [44-47]. There has been a growing interest in new electro-conductive polymer materials which feature smart characteristics that can be manipulated by, for example, external magnetic fields. These materials are increasingly being utilized in coating manufacturing processes. In view of these applications, the current article examines the *convective-radiative magnetohydrodynamic non-*

Newtonian second grade fluid boundary layer flow from a curved stretching surface under a static radial magnetic field. A further novelty of the present model is that it also includes Ohmic heating and viscous dissipation effects in the thermal analysis and furthermore a velocity slip condition at the sheet surface (wall). The transformed conservation boundary layer equations are solved numerically with an appropriate Runge-Kutta technique. The numerical solutions are verified with special cases from the literature. Contour plots for streamlines and isotherms are visualized and analyzed. The impact of emerging parameters on velocity and temperature distributions is evaluated in detail. Skin friction and Nusselt number are also computed.

2. Mathematical Model

Steady two-dimensional (2D) hydromagnetic flow of a non-Newtonian second grade fluid (magnetic polymer) from a curved stretching surface of radius R is considered. Here the problem is modeled based on curvilinear coordinates (r, s). The energy equation features thermal radiation, Joule heating and viscous dissipation. First order velocity slip is also included in the boundary conditions, since polymers are known to exhibit slip phenomena. It is assumed that the constant magnetic field (B_0) acts normal to the curved surface, applied in the radial direction. Unidirectional radiative flux acts transverse to the curved surface. The magnetic polymer is assumed to be optically thick, and the Rosseland diffusion approximation is deployed. Hall current and magnetic induction effects are neglected. The physical configuration is shown in **Fig.1**. It is assumed that the surface is stretched with a velocity, $u_w = U_{slip} + as$, where a is a positive constant. Based on the assumptions mentioned, the governing equations (continuity, momentum and energy) are obtained by extending the models in [5,12,18,21] for the second-grade viscoelastic fluid:

$$\frac{\partial}{\partial r}\big((r+R)v\big) + R\frac{\partial u}{\partial s} = 0, \tag{1}$$

$$\frac{1}{r+R}u^2 = -\frac{1}{\rho}\frac{\partial p}{\partial r}\ , \tag{2}$$

$$v\frac{\partial u}{\partial r}+\frac{uR}{r+R}\frac{\partial u}{\partial s}+\frac{uv}{r+R}$$
$$=-\frac{1}{\rho}\frac{R}{r+R}\frac{\partial p}{\partial s}+\nu\left(\frac{\partial^2 u}{\partial r^2}+\frac{1}{r+R}\frac{\partial u}{\partial r}-\frac{u}{(r+R)^2}\right)$$
$$+\frac{\alpha_1}{\rho}\left[\frac{2}{r+R}\frac{\partial^2 u}{\partial r^2}\frac{\partial u}{\partial s}-\frac{2}{(r+R)^2}\frac{\partial u}{\partial s}\frac{\partial u}{\partial r}+\frac{2}{r+R}\frac{\partial v}{\partial s}\frac{\partial u}{\partial r}+\frac{2}{r+R}v\frac{\partial^2 u}{\partial r^2}\right.$$
$$\left.-\frac{2}{(r+R)^2}v\frac{\partial u}{\partial r}-\frac{4R}{(r+R)^2}u\frac{\partial^2 u}{\partial s\partial r}-\frac{4R}{(r+R)^2}u\frac{\partial v}{\partial r}\frac{2R}{(r+R)^3}u\frac{\partial u}{\partial s}\right]-\frac{\sigma}{\rho}B_0^2 u \quad (3)$$

$$v\frac{\partial T}{\partial r}+\frac{uR}{r+R}\frac{\partial T}{\partial s}=\frac{k}{(\rho c_p)}\left(1+\frac{16\sigma^*}{3kk^*}\right)\left(\frac{1}{r+R}\frac{\partial T}{\partial r}+\frac{\partial^2 T}{\partial r^2}\right)+\frac{\mu}{(\rho c_p)}\left(\frac{\partial u}{\partial r}+\frac{u}{r+R}\right)^2+\frac{\sigma B_0^2}{(\rho c_p)}u^2 \quad (4)$$

The associated boundary conditions at the curved sheet surface and in the free stream are prescribed as follows:

$$u=l\left(\frac{\partial u}{\partial r}\right)+as,\ \ v=0,\ \ T=T_w \quad at\ r=0,$$
$$u\to 0,\ \ \frac{\partial u}{\partial r}\to 0,\ \ T\to T_\infty \quad as \quad r\to\infty \quad (5)$$

where $U_{slip}=l\left(\frac{\partial u}{\partial r}\right)$.

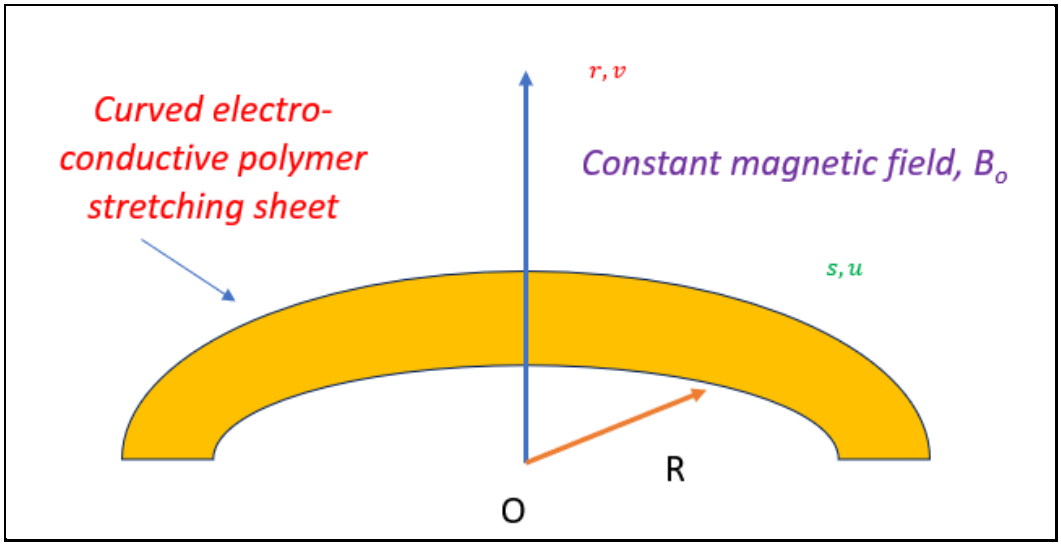

Fig.1. Geometric flow configuration

Defining the following transformations to normalize the governing equations [3,5,12]:

$$u=as,f'=(\eta),v=\frac{R}{r+R}\sqrt{av_f}\,f(\eta),\zeta=\sqrt{\frac{a}{v}}r,\ \ p=\rho_f a^2 s^2 P(\zeta),\theta(\eta)=\frac{T-T_\infty}{T_w-T_\infty} \quad (6)$$

Introducing equation (6) in Equations (1) to (5), we have the following similarity equations for pressure, velocity and temperature:

$$P' = \frac{f'^2}{(\zeta+K)}, \tag{7}$$

$$\frac{2K}{(\zeta+K)}P = f''' + \frac{1}{(\zeta+K)}f'' - \frac{1}{(\zeta+K)^2}f' - \frac{K}{(\zeta+K)}f'^2 + \frac{1}{(\zeta+K)}ff'' + \frac{K}{(\zeta+K)^2}ff' + \Gamma\left[\frac{2K}{\zeta+K}f'f''' - \frac{2K}{(\zeta+K)^2}f'f''' - \frac{8K}{(\zeta+K)^2}f'f'' + \frac{4K}{(\zeta+K)^3}f'f'' + \frac{6K}{(\zeta+K)^3}f'^2 - \frac{4K}{(\zeta+K)^4}ff'\right] - Mf', \tag{8}$$

$$(1+Rd)\left(\theta'' + \frac{1}{(\zeta+K)}\theta'\right) + Pr\frac{K}{(\zeta+K)}f\theta' Br\left(f" + \frac{1}{(\zeta+K)}f'\right)^2 + MBrf'^2 = 0, \tag{9}$$

The transformed associated boundary conditions emerge as:

$$f(\zeta) = 0, f'(\zeta) = 1 + Lf''(\zeta), \quad \theta(\zeta) = 1, at \quad \zeta = 0$$
$$f'(\zeta) = 0, \quad f''(\zeta) = 0, \ \theta(\zeta) = 0 \qquad as \quad \zeta \to 0 \tag{10}$$

Here the following dimensionless variables are defined:

$$K = \sqrt{\frac{a}{v}}R, M = \frac{\sigma B_0^2}{\rho a}, \Gamma = \frac{\alpha_1 a}{\mu}, Pr = \frac{v}{\alpha}, Rd = \frac{16\sigma^* T_\infty^3}{3kk^*}, Ec = \frac{a^2 s^2}{c_p(T_w - T_\infty)}, Br = PrEc, \ L = l\sqrt{\frac{a}{v}} \tag{11}$$

These denote respectively the curvature parameter, magnetic field parameter, second grade viscoelastic fluid parameter, Prandtl number, radiation parameter, Eckert number, Brinkman number and velocity slip parameter.

By neglecting the pressure from momentum Equation (8) using Equation (7), the momentum Equation (8) emerges as:

$$f^{iv} + \frac{2}{(\zeta+K)}f''' - \frac{1}{(\zeta+K)}f'' + \frac{1}{(\zeta+K)}f' + \frac{K}{(\zeta+K)}(ff'' - f'f'') + \frac{K}{(\zeta+K)}(ff'' - f'^2) - \frac{K}{(\zeta+K)^3}ff' - M\left(f'' + \frac{1}{(\zeta+K)}f'\right) + 2\Gamma\left[\frac{K}{(\zeta+K)}f''f''' + \frac{K}{(\zeta+K)}f'^v f' - \frac{5K}{(\zeta+K)^3}f'f''' + \frac{12K}{(\zeta+K)^3}f'f'' + \frac{3K}{(\zeta+K)^3}ff''' - \frac{4K}{(\zeta+K)^3}f''^2 - \frac{6K}{(\zeta+K)^4}ff'' - \frac{8K}{(\zeta+K)^4}f'^2 + \frac{6K}{(\zeta+K)^5}ff'\right] = 0 \tag{12}$$

The prominent engineering quantities such as local skin-friction coefficient C_f and Nusselt number Nu are given by:

$$C_f = \frac{\tau_{rx}}{\frac{1}{2}\rho u_w^2} \tag{13}$$

$$Nu = \frac{xq_w}{k(T_w - T_\infty)}, \tag{14}$$

in which the shear stress τ_{rx} and heat flux q_w are defined respectively [9] as:

$$\tau_{rx} = \mu\left[\frac{\partial u}{\partial r} - \frac{u}{r+R} + \frac{2\alpha_1}{\mu}\left\{\frac{R}{r+R}\frac{\partial u}{\partial r}\frac{\partial u}{\partial x} + \frac{v}{r+R}\frac{\partial u}{\partial r} - \frac{2Ru}{(r+R)^2}\frac{\partial u}{\partial x} - \frac{2uv}{(r+R)^2}\right\}\right]_{r=0}, \tag{15}$$

$$q_w = \left(k + \frac{16\sigma^* T_\infty^3}{3k^*}\right)\frac{\partial T}{\partial r}\Big|_{r=0}, \quad (16)$$

With the help of Equation (6), equations (13) and (14) are transformed to:

$$C_f (Re_x)^{1/2} = 2\left[f''(0)\frac{f'(0)}{K} + \Gamma\left\{f'(0)f''(0) - \frac{2}{K}\left(f'(0)\right)^2\right\}\right], \quad (17)$$

$$Nu(Re_x)^{-1/2} = -(1+Rd)\theta'(0) \quad (18)$$

Here $(Re_x)^{1/2} = \sqrt{\frac{a}{v}}s$ is the Local Reynolds number.

3. Numerical Solution:

To derive closed form solutions of the final dimensionless differential equations (9) and (12) subject to the boundary conditions (10) is difficult, if not intractable. Therefore, these equations are solved by employing the Runge-Kutta numerical approach along with a shooting scheme in MATLAB symbolic software and the procedure is as follows:

$$f = y_1, f' = y_2, f'' = y_3, f''' = y_4, \quad (19)$$

$$y_4' = -\frac{1}{\left(1+\frac{K}{(\zeta+K)}y_2\right)}\left[\frac{2}{(\zeta+K)}y_4 - \frac{1}{(\zeta+K)}y_3 + \frac{1}{(\zeta+K)}y_2 + \frac{K}{(\zeta+K)}(y_1y_3 - y_2y_3) + \right.$$

$$\frac{K}{(\zeta+K)}(y_1y_3 - y_2^2) - \frac{K}{(\zeta+K)^3}y_1y_2 - M\left(y_3 + \frac{1}{(\zeta+K)}y_2\right) + 2\Gamma\left[\frac{K}{(\zeta+K)}y_2y_3 - \frac{5K}{(\zeta+K)^3}y_2y_4 + \right.$$

$$\left.\left.\frac{12K}{(\zeta+K)^3}y_2y_3 + \frac{3K}{(\zeta+K)^3}y_1y_4 - \frac{4K}{(\zeta+K)^3}y_3^2 - \frac{6K}{(\zeta+K)^4}y_1y_3 - \frac{8K}{(\zeta+K)^4}y_2^2 + \frac{6K}{(\zeta+K)^5}y_1y_2\right]\right] \quad (20)$$

$$\theta = y_5, \ \theta' = y_6, \quad (21)$$

$$\theta'' = -\frac{1}{(1+Rd)}\left[\frac{1}{(\zeta+K)}\theta' + Pr\frac{K}{(\zeta+K)}f\theta' Br\left(f'' + \frac{1}{(\zeta+K)}f'\right)^2 + MBrf'^2\right] \quad (22)$$

The transformed boundary conditions are:

$$y_1(0) = 0, \ y_2(0) = 1 + L\, y_3(0), \quad y_5(0) = 1$$

$$y_2(\infty) = 1, \quad y_3(\infty) = 0, \ y_5(\infty) = 0 \quad (23)$$

4. Validation of numerical solutions

In order to validate the obtained Runge-Kutta numerical solution, a comparative study of friction factor (skin friction) versus curvature parameter K is conducted. Solutions are compared with those from the literature for special cases where viscous heating is absent (*Ec* = 0), second grade viscoelastic fluid parameter is neglected ($\Gamma = 0$) and wall velocity slip is absent (L = 0). The special reduced cases correspond to the earlier studies of Sajid *et al.* [3], Abbas *et al.* [4] and Hayat *et al.* [15]. The comparisons are shown in **Table 1**.

Table1: Comparison of the friction factor for the curvature parameter K with $L = \Gamma = \mathrm{Ec} = 0$.

K	Ref. [3]	Ref. [4]	Ref. [15]	Present R-K results
5	0.75763	0.75754	0.75762	0.757642
10	0.87349	0.87480	0.87350	0.874823
20	0.93561	0.93564	0.93562	0.935612
30	0.95686	0.95685	0.95685	0.956867

From this, it is observed that the friction factor is boosted for higher K i. e. as the sheet becomes progressively flatter. Excellent correlation between the present Runge-Kutta numerical results and those in the literature has been achieved. Confidence in the present numerical approach is therefore justifiably very high.

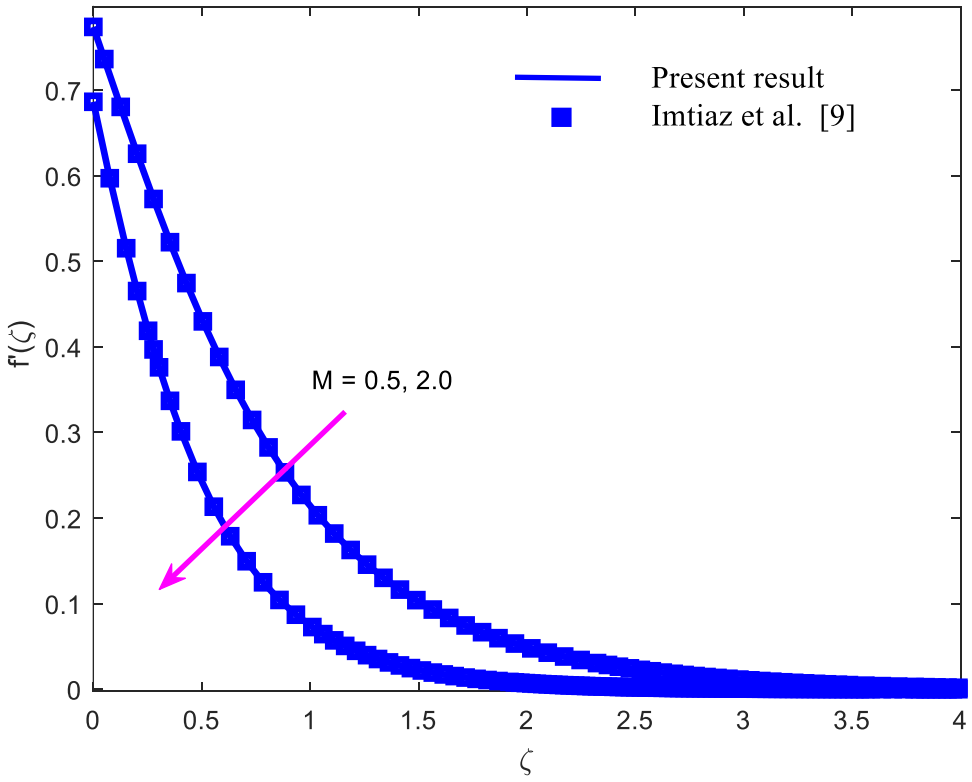

Fig.2. Comparison graph for validation of code.

Furthermore, in order to validate the employed computer code, the effect of magnetic field parameter Mon velocity function for the second-grade non-Newtonian fluid is benchmarked with the solution of Imtiaz *et al.* [9] and the comparison is displayed in Fig.2. It is evident that excellent agreement between the present results and previous published work [9] is achieved confirming high confidence in the present numerical results.

4. Graphical description

The main focus of the current investigation is to examine both the streamline and isotherm distributions and velocity and temperature profiles in non-Newtonian dissipative radiative second grade fluid flow from a curved stretching surface with wall slip. For the numerical calculations, the parameter values considered of the present study are : $K = 2.2$, $M = 2.2$, $\Gamma = 0.8$ (non-Newtonian fluid), $\Gamma = 0.0$ (Newtonian fluid), $Rd = 2.2$, $Pr = 4.4$, $Br = 2.2$, $L = 0.2$. The effects of all key emerging parameters on streamline contours, isotherm contours, velocity and temperature are visualized in graphical plots (**Figs. 3-13**).

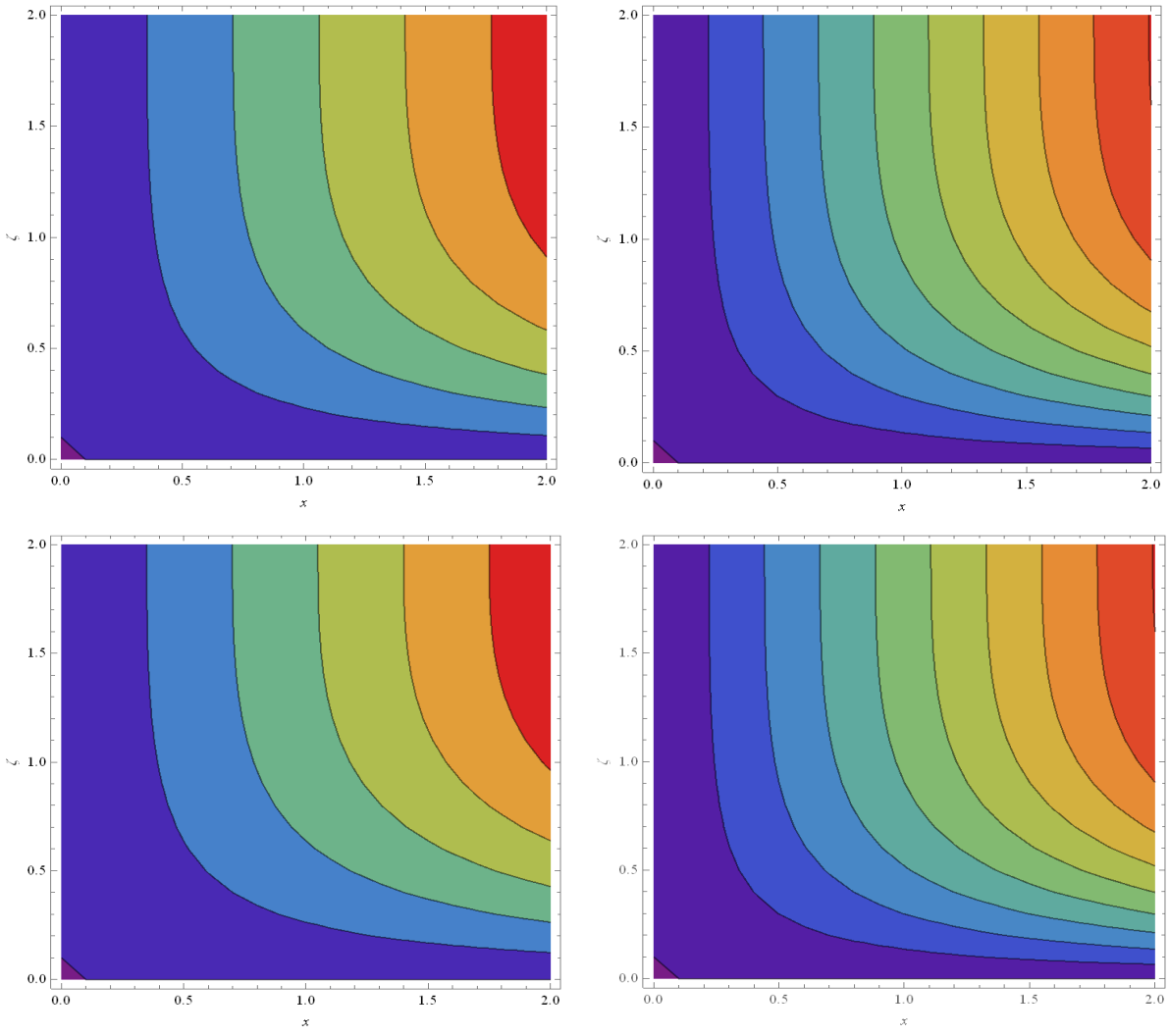

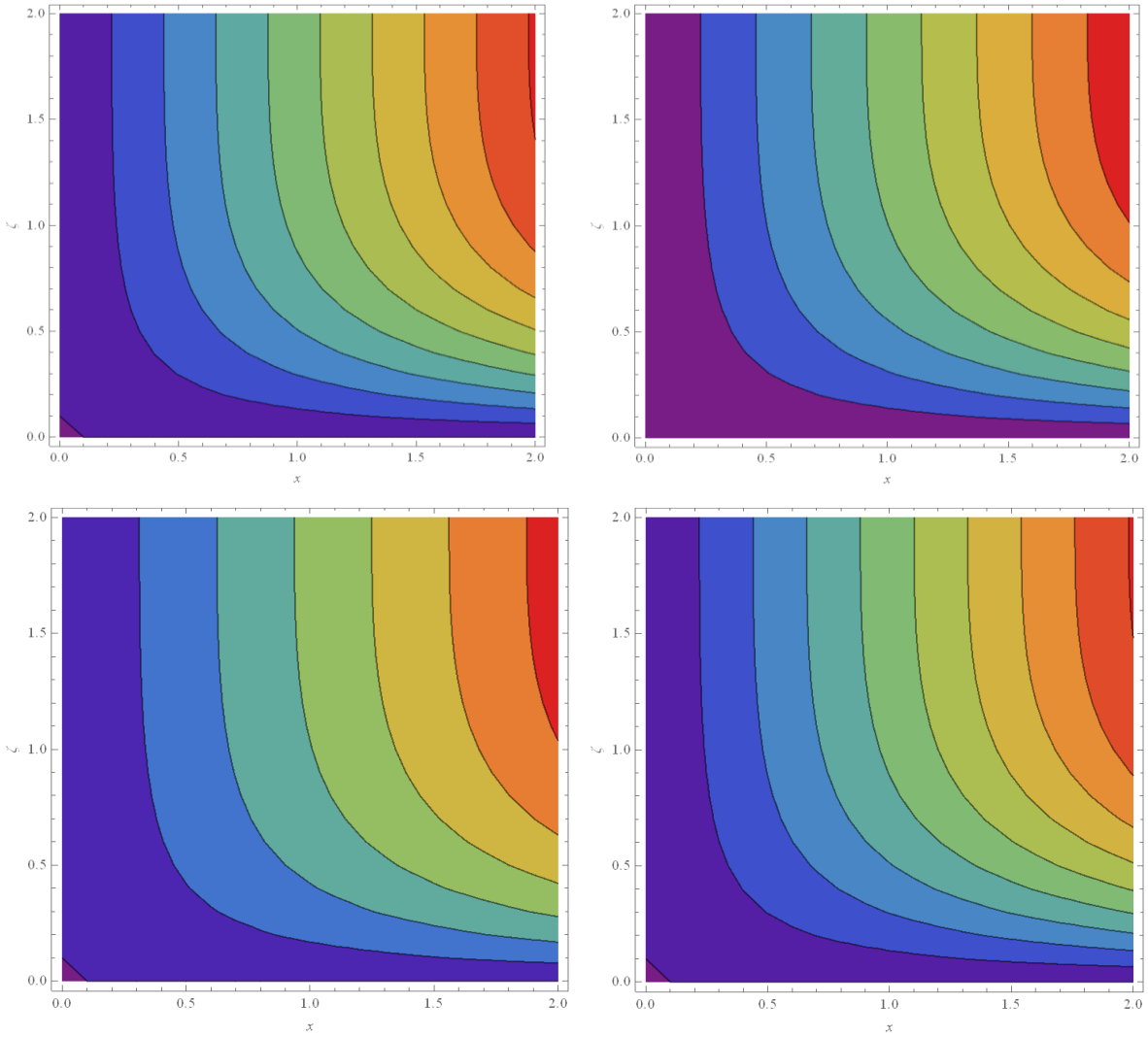

Fig.3. Contour plots for streamlines (a) $L = 0.01$ (b) $L = 0.2$ (c) $M = 0.2$ (d) $M = 2.0$ (e) $K = 2.0$ (f) $K = 6.0$ (g) $\Gamma = 0.0$ (h) $\Gamma = 0.8$

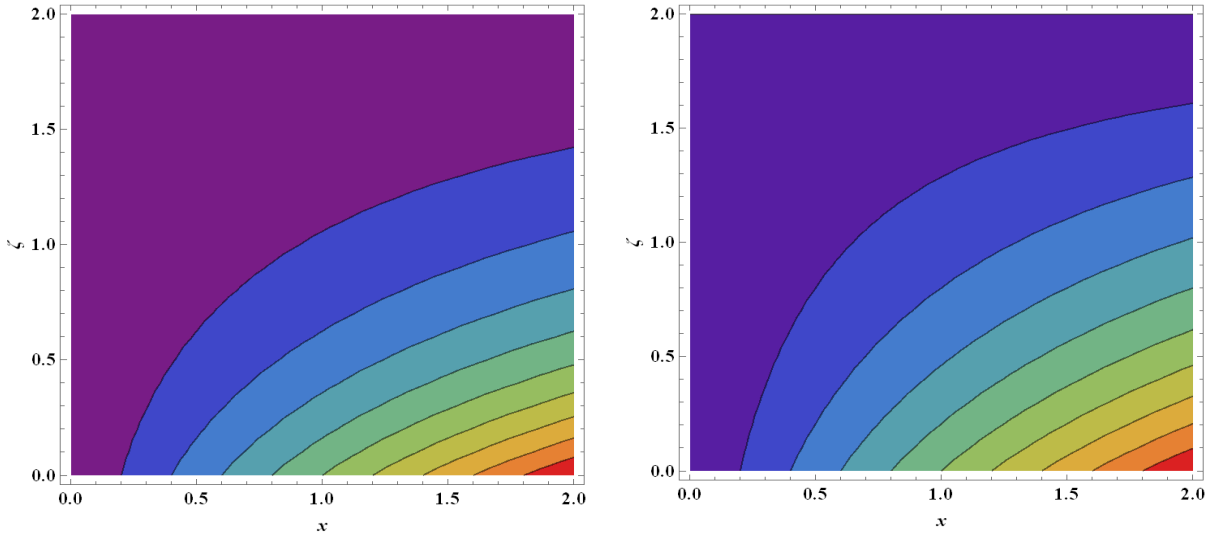

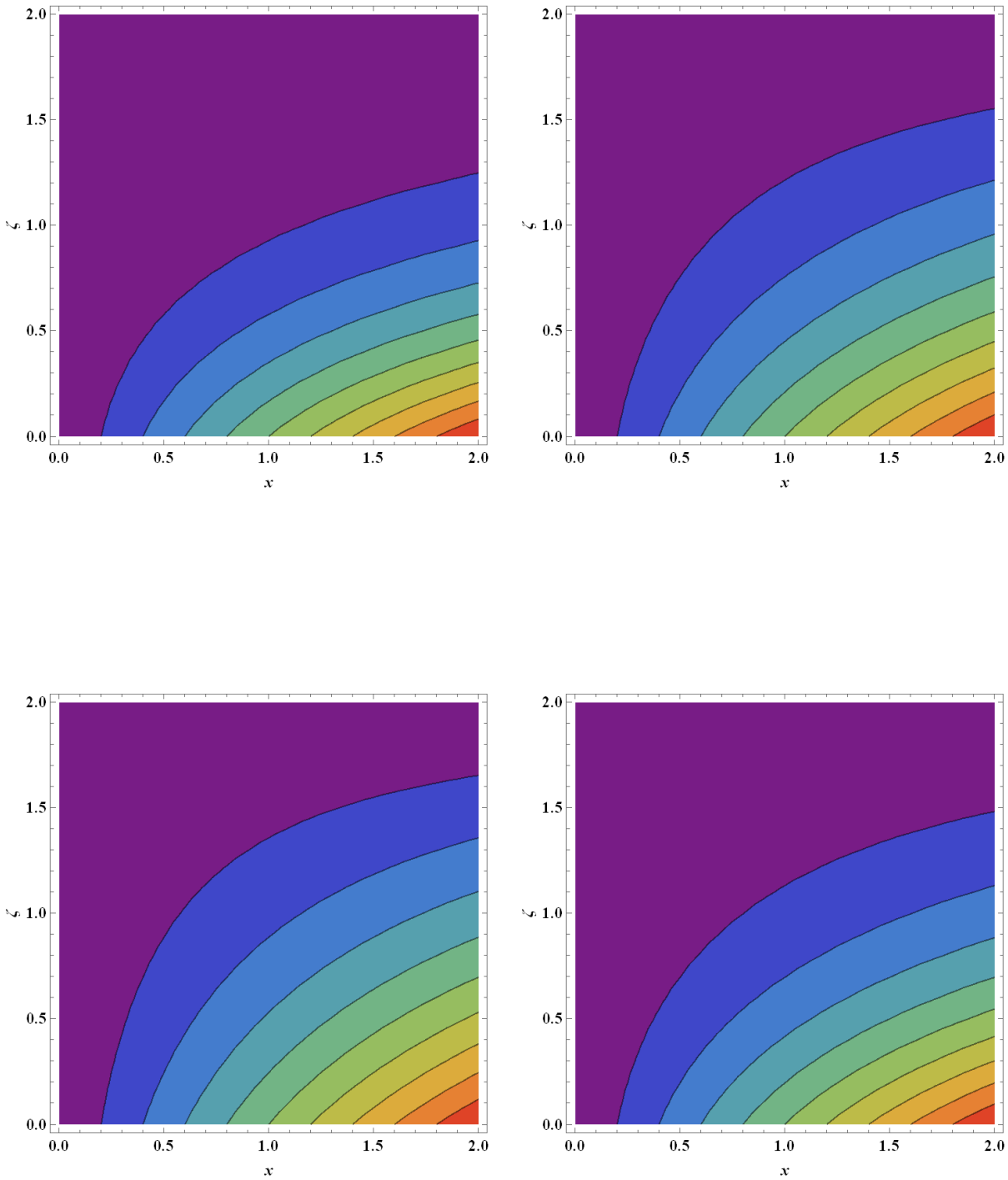

Fig.4. Contour plots for isotherms (a) $Rd = 0.6, \Gamma = 0.0$ (b) $Rd = 2.0, \Gamma = 0.0$ (c) $Rd = 0.6, \Gamma = 0.8$ (d) $Rd = 2.0, \Gamma = 0.8$ (e) $Br = 0.6, \Gamma = 0.8$ (f) $Br = 2.0, \Gamma = 0.8$

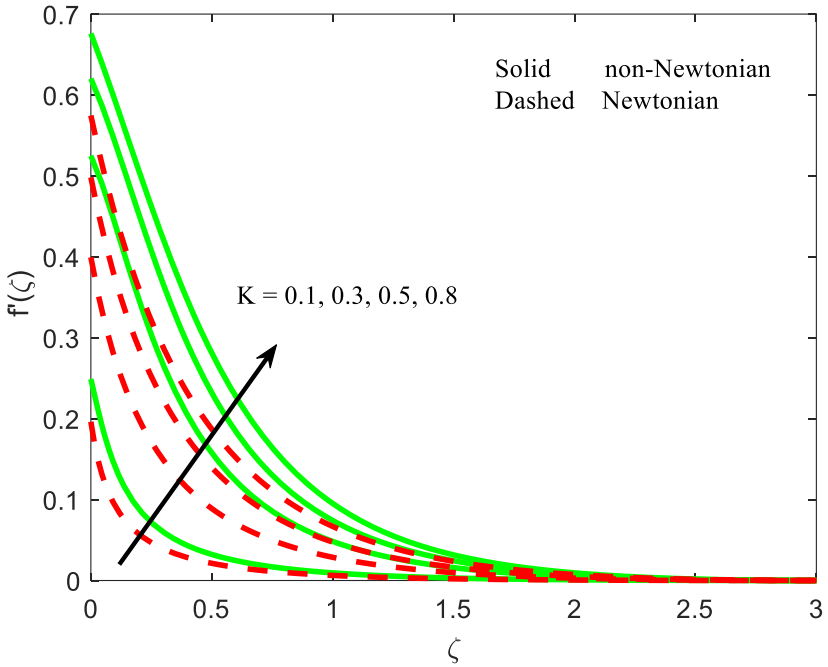

Fig 5. Variation in $f'(\zeta)$ with K.

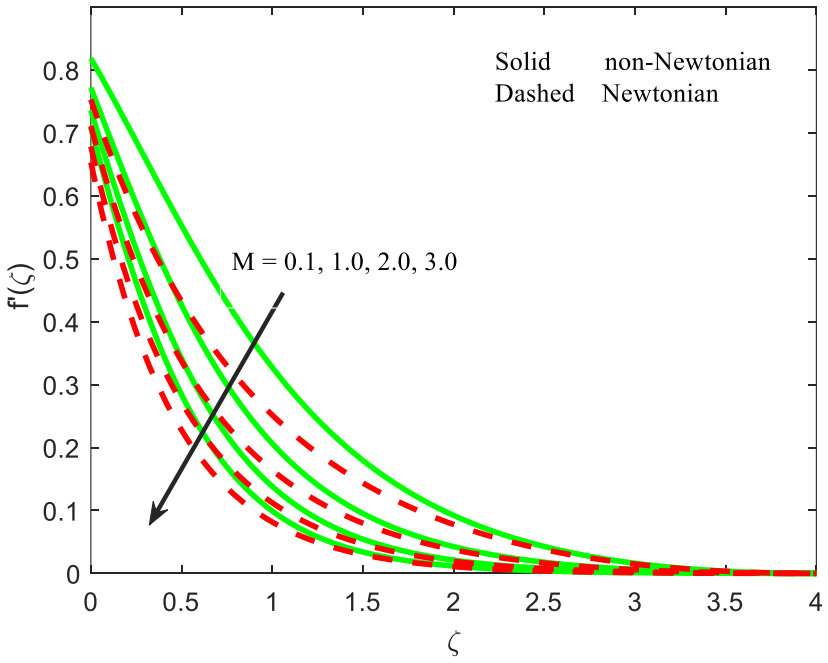

Fig 6. Variation in $f'(\zeta)$ with M.

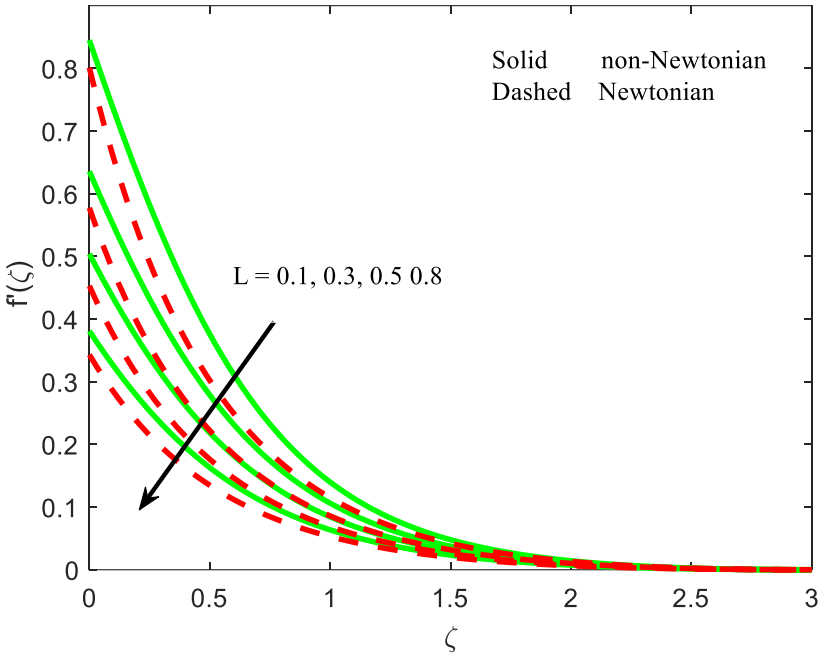

Fig 7. Variation in $f'(\zeta)$ with L.

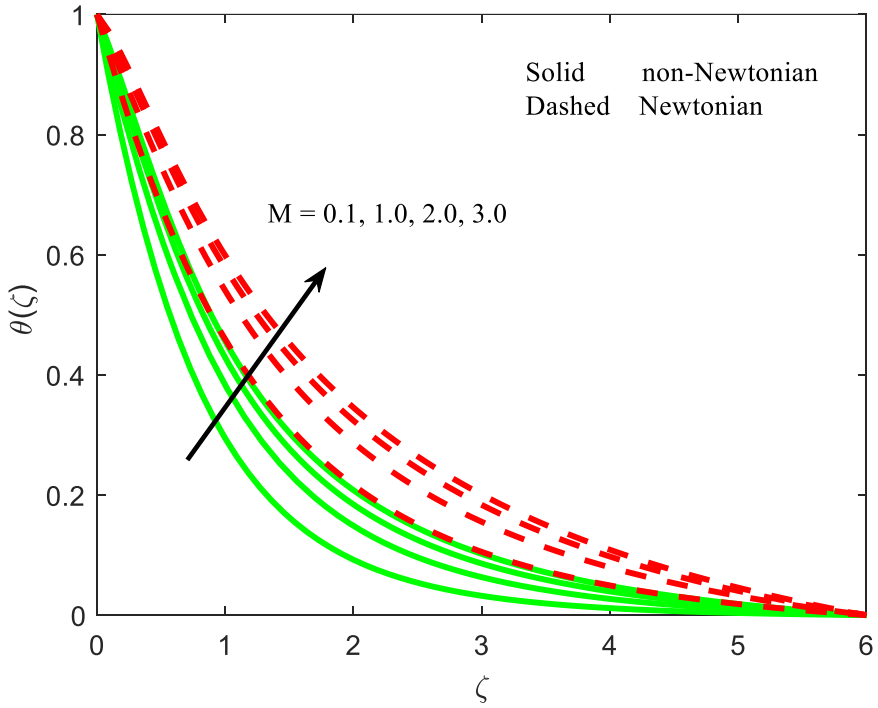

Fig 8. Variation in θ with M.

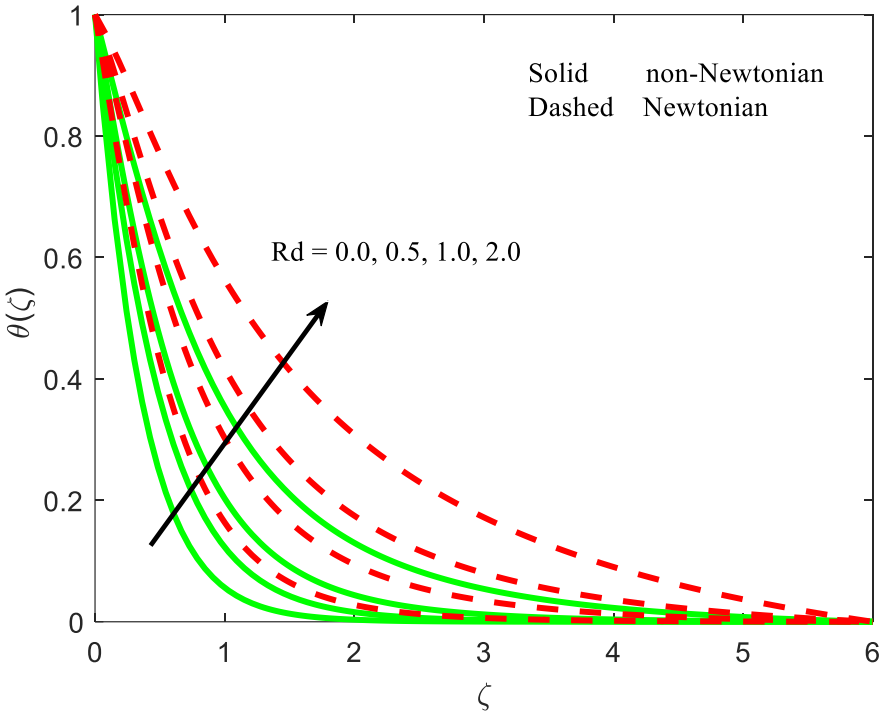

Fig 9. Variation in θ with Rd.

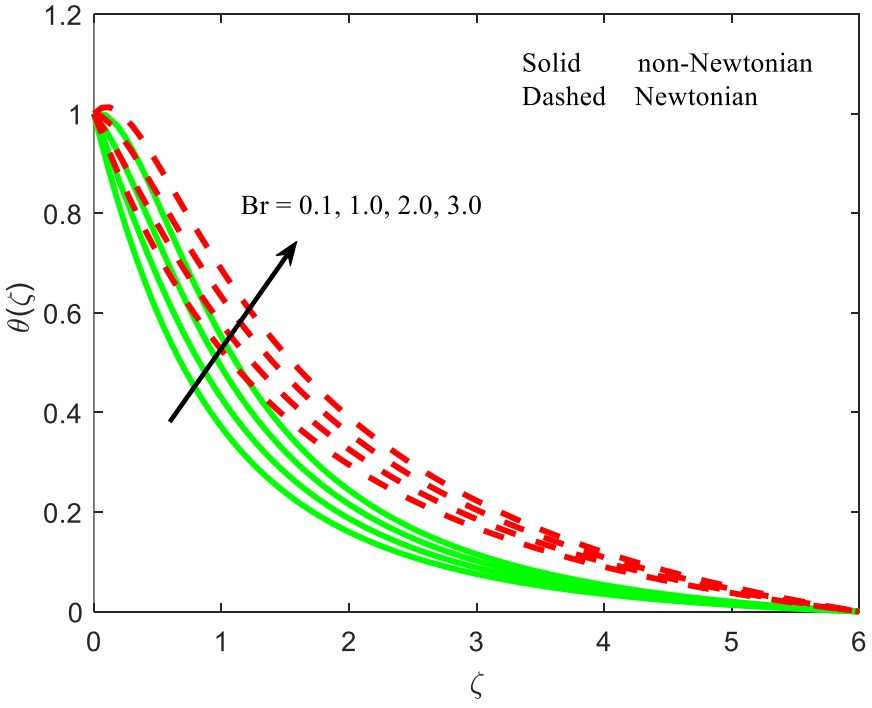

Fig 10. Variation in θ with Br.

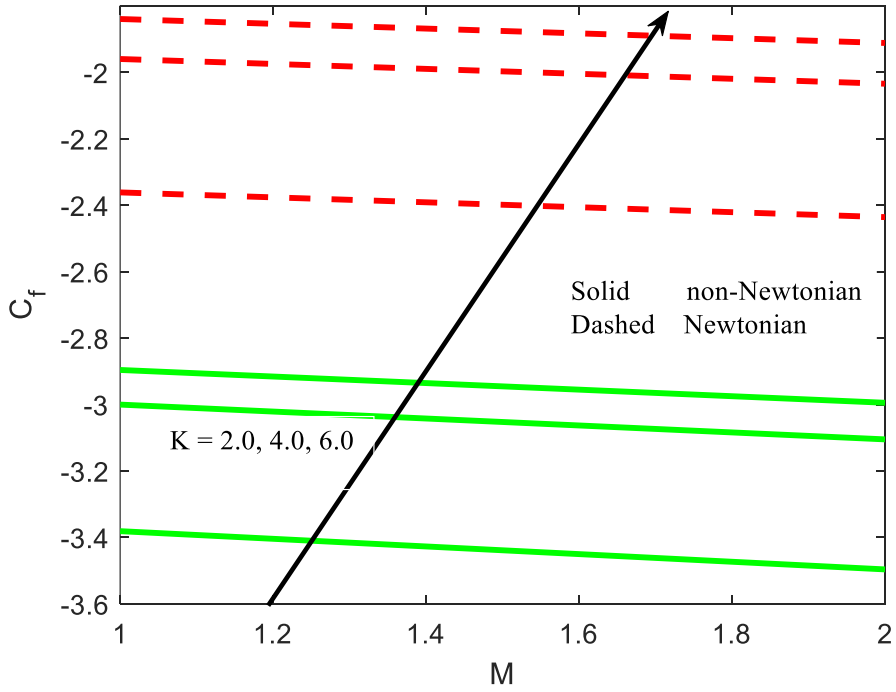

Fig 11. Variation in C_f with K.

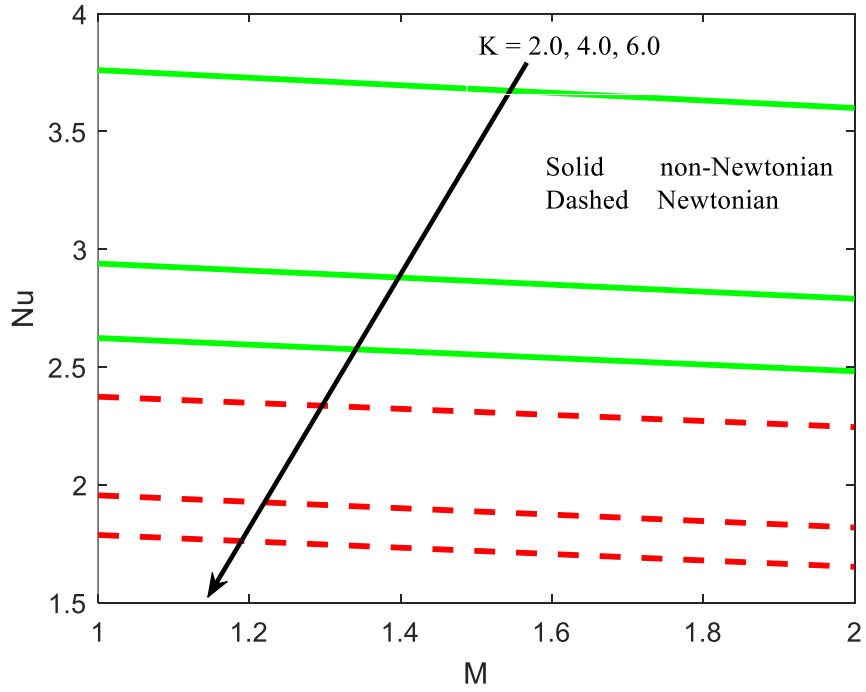

Fig 12. Variation in Nu with K.

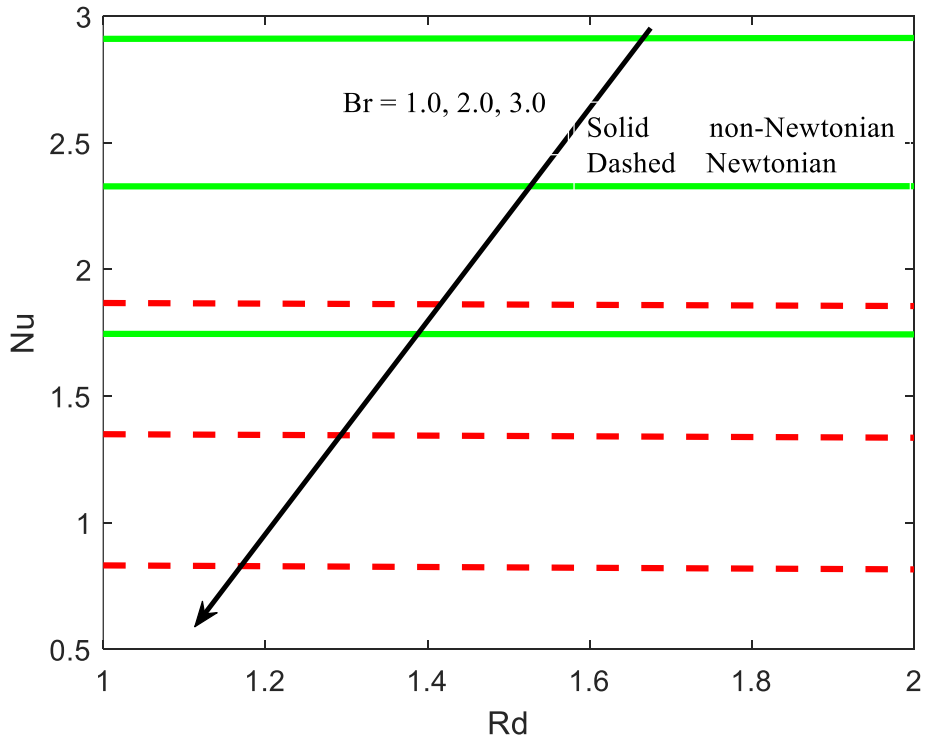

Fig 13. Variation in Nu with Br.

4.1. Streamlines

The contour plots for streamlines with variation in different flow parameters such as velocity slip parameter L, magnetic variable M, curvature parameter K, non-Newtonian fluid parameter Γ have been displayed in Figs. 3(a)-3(h) respectively. The influence of increasing velocity slip parameter L on streamlines (Figs. 3(a) and 3(b)) is to constrict the higher velocity (top right) zone. In other words, the flow is decelerated with greater velocity slip and there is the emergence of lower velocity (graded blue) zones in the left of the plot. A similar effect is induced with increasing magnetic parameter (M) which constricts the bands of streamlines ((Figs. 3(c) and 3(d)). Lower velocity zones emerge due to the strong deceleration associated with the magnetic force. The boundary layer flow is therefore significantly damped with stronger magnetic field and the initial larger red, orange and yellow higher velocity zones for M = 0.2 (left plot) are considerably contracted for M = 2.0 (right plot). Figs. 3(e) & 3(f)) indicate that streamlines are also suppressed with a boost in the curvature from $K = 2.0$ to $K = 6.0$. As the curved sheet tends to a flatter geometry (higher K values), the velocity is reduced, and the higher velocity red zone is contacted. Much lower velocity zones (purple) also emerge at the left of the plot indicating strong retardation in the boundary layer flow. Figs. 3(g) and 3(h) show that streamline magnitudes are suppressed for the case of the non-

Newtonian second grade fluid ($\Gamma = 0.8$) as compared to the Newtonian fluid ($\Gamma = 0$). The presence of viscoelasticity influences the tensile stresses in the magnetic polymer. Viscous effects also become dominant, and this decelerates the flow relative to the Newtonian case. More graded blue minimal velocity zones therefore appear only in the non-Newtonian case (right plot) and are less in number in the Newtonian case (left plot). The green, orange, yellow and red zones (higher velocity) are significantly depleted in the non-Newtonian case (right plot). The incorporation of a robust viscoelastic model in the model is therefore justified since the classical Newtonian case *over-predicts* the streamline magnitudes throughout the domain.

4.2. Isotherms

The isotherm patterns with variation in selected parameters are displayed in Figs. 4(a)-4(f) respectively. Figs. 4(a) & 4(b) show the isotherm contour plots for different thermal radiation parameter Rd for the Newtonian fluid case ($\Gamma = 0$). It is perceived that the temperature function is escalating for higher thermal radiation since the higher temperature zones become contracted in the right plot (Rd = 0). The impact of radiation on temperature function for the case of second grade fluid is elucidated in Figs. 4(c) & 4(d). The influence of thermal radiation is smaller for the non-Newtonian fluid case as compared to the Newtonian fluid. However, temperatures are still greater than for the non-radiative case (Rd =0). Radiative flux energizes the boundary layer regime and encourages thermal diffusion. This leads to an increase in temperatures (lighter purple zones compared with darker purple zones) and higher thermal boundary layer thickness. The impact of Brinkman number Br on the isotherms has been displayed in Figs. 4(e) and 4(f) for non-Newtonian second grade fluid. The temperature isotherms are reduced for larger Brinkman number and the associated thermal boundary layer thickness is also reduced (larger cooler purple zones emerge for Br = 2.0 compared with Br = 0.8). Br features in both the viscous dissipation and Ohmic dissipation terms in the transformed energy equation (9) i. e. $+Pr\frac{K}{(\zeta+K)}f\theta' Br\left(f'' + \frac{1}{(\zeta+K)}f'\right)^2 + MBrf'^2$. Since non-zero magnetic field is applied, the Ohmic heating (Joule dissipation) will also contribute to the re-distribution of thermal energy in the boundary layer. Clearly dissipative effects will modify the heat transfer in the boundary layer and are important to include in realistic models of magnetic polymer flows. In addition, the temperature magnitudes overall in the boundary layer on the curved surface are smaller for the second-grade fluid ($\Gamma = 0.8$) whereas as they are greater for the Newtonian fluid ($\Gamma = 0$). The implication is that the rheological (viscoelastic)

characteristic of the magnetic polymer achieves a cooling effect which is advantageous in coating operations.

4.3. Velocity field

Fig. 5 is plotted to examine the impact of curvature parameter Kon velocity function, $f'(\varsigma)$. It is evident that the viscous force is reduced with greater curvature parameter K (i. e. tendency towards a flatter sheet) and momentum development is assisted, leading to flow acceleration. In the case of infinite curvature, a flat stretching sheet is obtained (infinite radius scenario). The trends computed in Fig. 5 concur with the earlier studies reported in [5] and [21]. Also, it is evident that that the velocity computed for Newtonian fluid $(\Gamma = 0)$ is lower as compared to second grade fluid (non-Newtonian fluid). This is associated with the greater viscous effect and upsurge in flow resistance in the non-Newtonian fluid which induces boundary layer deceleration and an increase in momentum boundary layer thickness. In addition, the momentum boundary layer thickness is reduced for larger curvature parameter, K.

Fig. 6 shows the evolution in velocity profile with magnetic parameter, M. Significant depletion in velocity is generated with an increase in magnetic field. The Lorentz force appears in the reduced momentum boundary layer Eqn. (12) as $-M\left(f'' + \frac{1}{(\zeta+K)}f'\right)$ and is clearly a retarding body force. It acts in the reverse direction to the flow and retards the boundary layer flow on the curved surface, increasing hydrodynamic boundary layer thickness. Furthermore, the velocity magnitudes for non-Newtonian fluid are consistently higher than Newtonian fluid indicating that the magnetic field exerts a reduced effect on the magnetic polymer. Flow reversal is however never induced in the regime since velocity magnitudes are positive at all locations transverse to the curved surface.

Fig. 7 visualizes the distribution of fluid velocity $f'(\varsigma)$ for various values of velocity slip parameter, L again for both second grade viscoelastic fluid and Newtonian fluid. While an increment in slip diminishes both fluid velocities, the non-Newtonian fluid again achieves higher velocity magnitudes. The deceleration is more prominent in the Newtonian fluid which will correspond to a thicker momentum boundary layer than the non-Newtonian fluid. The velocity slip is simulated in the augmented wall boundary condition, $f'(\zeta) = 1 + Lf''(\zeta)$, in Eqn. (10). Velocity is therefore also modified via the slip effect by the shear rate at the wall. Increment in L therefore induces a delay in the boundary layer response which manifests in deceleration in the flow. As anticipated the primary effect is at the curved sheet surface (wall) and then decays progressively into the boundary layer. Again, back flow is never generated in

the regime as velocity magnitudes never become negative, irrespective of magnetic field parameter value. The inhibiting effect of external magnetic field is therefore clearly demonstrated, and this non-intrusive method provides an excellent mechanism for manipulating flow characteristics in electro-conductive polymer materials processing [46, 47].

4.4. Fluid Temperature

Fig.8 displays the variations of magnetic variable M on temperature distribution. It is apparent that a strong escalation in temperature is induced with greater applied magnetic field. The parameter M features in the Ohmic dissipation term in the thermal boundary layer Eqn. (9), viz, $+MBrf'^2$. The temperature field is also modified indirectly by the Lorentzian body force term in the momentum Eqn. (12) via this Ohmic term and additionally the other higher order terms $+Pr\frac{K}{(\zeta+K)}f\theta'Br\left(f''+\frac{1}{(\zeta+K)}f'\right)^2$ in Eqn. (9). The supplementary work expended in dragging the magnetic polymer against the action of the radial magnetic field (Lorentz body force) is dissipated as thermal energy. This energizes the fluid and boosts temperature and also thermal boundary layer thickness. Furthermore, the Ohmic dissipation is accentuated with higher magnetic parameter, and this also results in further heating of the fluid. A dual contribution of the magnetic field is therefore sustained leading to significant heating in the boundary layer regime. It is also noteworthy that the non-Newtonian second grade fluid achieve lower temperatures relative to the Newtonian fluid. The viscoelastic characteristics of real magnetic non-Newtonian polymers have been confirmed to achieve improved temperature control in coating applications as elaborated by Kashevskii *et al.* [46] and Kimura [47]. Again, the inclusion of non-Newtonian characteristics (stress relaxation and retardation are featured in the second-grade model) in the current analysis for simulating more realistically actual electroconductive polymer flows is therefore clearly justified.

Fig.9 depicts the response in temperature with a change in radiation parameter, Rd, again for both Newtonian and non-Newtonian fluid cases. Cleary, stronger radiative flux boosts the temperature significantly. The radiative parameter features in the augmented thermal diffusion term, $(1+Rd)\left(\theta''+\frac{1}{(\zeta+K)}\theta'\right)$ in Eqn. (9). When radiative flux is absent i.e. for purely convective-conductive boundary layer flow, $Rd = 0$ and temperatures are minimized for both Newtonian and non-Newtonian fluids. The presence of radiative flux strongly energizes the boundary layer and encourages thermal diffusion. This heats the regime and enhances thermal boundary layer thickness. Temperature $\theta(\varsigma)$ is therefore hiked. A similar trend is observed in

other studies in the literature including Hayat *et al.* [22] and Riaz *et al.* [25], who have also deployed the Rosseland diffusion flux model. It is also evident that lower temperatures are produced for the non-Newtonian liquid (magnetic polymer) relative to the Newtonian fluid, again confirming that improved temperature control is achieved with a rheological polymer which is not captured in the Newtonian classical model (Γ=0 for absence of second grade viscoelasticity). The thermal boundary layer thickness of the Newtonian fluid will as such be significantly higher than the non-Newtonian fluid.

Fig.10. presents the impact of Brinkman number Br on temperature field, $\theta(\varsigma)$. It is found that temperature magnitudes are substantially boosted with augmentation in Br. Larger Brinkman number Brcorresponds to a boost in the kinetic energy dissipated by viscous heating in the regime. This escalates the thermal energy generation which in turn elevates the temperature magnitude and also thermal boundary layer thickness. Clearly the inclusion of the viscous heating effect is important in magnetic polymers. Neglection of this effect will under-predict actual temperatures. A stronger enhancement is computed for Newtonian fluid compared with non- Newtonian second-grade fluid, however, again confirming that magnetic non-Newtonian polymers achieve improved thermal control. It is also noteworthy that a slight temperature overshoot is produced at very high Brinkman number (*Br* = 3) in the Newtonian fluid case, in close proximity to the wall (curved surface) which is absent for the non-Newtonian case.

4.5. Friction factor and Nusselt number

Figs. 11-13 are plotted to illustrate the impact of curvature parameter, K, magnetic variable M and Brinkman number Br on skin friction factor C_f and Nusselt number Nu. It is observed that the friction factor is boosted for higher curvature whereas the Nusselt number is depleted with greater curvature parameter, *K*. Furthermore, the Nusselt number is a decreasing function of the Brinkman number (*Br*), since temperatures are elevated with the viscous dissipation effect. The heat transferred to the wall from the boundary layer will therefore be reduced. Overall, the non-Newtonian fluid achieves lower skin friction, but higher Nusselt number values are computed compared to the Newtonian fluid.

5. Conclusions

Motivated by coating flow processes utilizing magnetic rheological polymers, a mathematical model has been developed for *steady radiative magnetohydrodynamic non-Newtonian second grade fluid boundary layer flow from a curved stretching surface with Ohmic heating, viscous*

dissipation and velocity slip effects. The transformed similarity conservation boundary layer equations have been solved numerically with efficient Runge-Kutta quadrature and shooting techniques in MATLAB. The numerical solutions have been validated with special cases from the literature. Contour plots for streamlines and isotherms and velocity and temperature distributions have been visualized. The main findings of the current study may be summarized as follows:

1. The fluid velocity $f'(\varsigma)$ is boosted with greater higher curvature parameter, K, and momentum boundary layer thickness is reduced.
2. The velocity is a diminishing function of the velocity slip parameter, L. Higher slip parameter therefore decelerates the boundary layer flow and increases momentum boundary layer thickness on the curved surface.
3. Velocity is suppressed with increasing magnetic parameter whereas temperature is significantly boosted with magnetic field due to the dual effect of Ohmic dissipation and extra work expended in dragging the magnetic polymer against the magnetic field.
4. Higher velocity magnitudes and an associated thinner momentum boundary layer is produced for the viscoelastic (non-Newtonian i. e. $\Gamma \neq 0$) case relative to the Newtonian case ($\Gamma = 0$).
5. Lower temperatures and a thinner thermal boundary layer thickness are computed with increasing radiative parameter for the non-Newtonian liquid (magnetic polymer) relative to the Newtonian fluid, indicating that enhanced temperature control is achieved with viscoelastic electroconductive polymers.
6. Smaller temperature (and isotherm) magnitudes arise for the non-Newtonian second-grade fluid ($\Gamma = 0.8$) whereas greater magnitudes are computed for Newtonian fluid ($\Gamma = 0$).
7. Skin friction at the curved stretching surface is elevated with increasing curvature K (i.e. tendency towards a flatter surface) whereas Nusselt number is suppressed with greater curvature parameter, K.
8. A reduction in Nusselt number is observed with increasing viscous dissipation effect i. e. Brinkman number (Br).
9. Larger skin friction values are computed for the Newtonian fluid compared with the non-Newtonian fluid, whereas the opposite trend is observed for Nusselt number (heat transfer rate at the curved surface).

The present study has revealed some interesting insights into thermo-magnetic coating flows with electro-conductive polymers. Future studies may consider *unsteady* effects and a variety of *alternative non-Newtonian models* (e. g. Maxwell viscoelastic, Carreau, Cross or Oldroyd-B fluids) and will be communicated imminently.

References

[1] C. Kaplan, The flow of a compressible fluid past a curved surface, In: *Annual Report-National Advisory Committee for Aeronautics, USA.* 305 (1943) 752–773.

[2] L.J. Crane, Flow past a stretching plate, *Z. Angew. Math. Phys*. 21 (1970) 645–655.

[3] M. Sajid, N. Ali, T. Javed, Z Abbas, Stretching a curved surface in a viscous fluid, *Chin Phys Lett.* 27(2) (2010) 024703.

[4] Z. Abbas, M. Naveed, M. Sajid, Heat transfer analysis for stretching flow over a curved surface with magnetic field, *J. Engin. Thermophys*, 22 (2013) 337–345.

[5] T. Hayat et al., Darcy-Forchheimer flow due to a curved stretching surface with Cattaneo-Christov double diffusion: A numerical study, *Results in Physics*, 7, (2017) 2663-2670.

[6] C. Natalia Roşca, I. Pop, Unsteady boundary layer flow over a permeable curved stretching/shrinking surface, *European Journal of Mechanics B/Fluids*. 51 (2015) 61–67.

[7] N.F. Okechi, M. Jalil, S. Asghar, Flow of viscous fluid along an exponentially stretching curved surface, *Results in Physics*, 7 (2017) 2851–2854.

[8] K.M. Sanni, S. Asghar, M. Jalil, N.F. Okechi, Flow of viscous fluid along a nonlinearly stretching curved surface, *Results Phys*. 7 (2017) 1–4.

[9] M. Imtiaz, F. Mabood, T. Hayat, A.Alsaedi, Homogeneous-heterogeneous reactions in MHD radiative flow of second grade fluid due to a curved stretching surface, *Int. J. Heat and Mass Trans*. 145 (2019) 118781.

[10] S. Nadeem, M.R. Khan, A.U. Khan, MHD stagnation point flow of viscous nanofluid over a curved surface, *Phys. Scripta* 94 (11) (2019) 115207.

[11] T. Hayat, S. Qayyuma, A. Alsaedi, B.Ahmad, Entropy generation minimization: Darcy-Forchheimer nanofluid flow due to curved stretching sheet with partial slip, *Int. Commun. Heat and Mass Trans.* 111 (2020) 104445.

[12] R. Raza, F. Mabood, R. Naz, S. I. Abdelsalam, Thermal transport of radiative Williamson fluid over stretchable curved surface, Thermal Science and Engineering Progress, 23, (2021), 100887.

[13] T. Hayat, A. Aziz, T. Muhammad, A. Alsaedi, Numerical study for nanofluid flow due to a nonlinear curved stretching surface with convective heat and mass conditions, *Results in Phys.* 7 (2017) 3100–3106.

[14] T. Hayat, F. Haider, T. Muhammad, A. Alsaedi, Numerical study for Darcy Forchheimer flow of nanofluid due to an exponentially stretching curved surface. *Results in Phys*. 8 (2018) 764–771.

[15] T.Hayat, S. Qayyum, A. Alsaedi, B. Ahmad, Entropy generation minimization: Darcy-Forchheimer nanofluid flow due to curved stretching sheet with partial slip. *Int. Comm. Heat Mass Transf.* 111 (2020) 104445.

[16] M.R. Khan, Numerical analysis of oblique stagnation point flow of nanofluid over a curved stretching/shrinking surface, *Phys. Scripta*, 95 (10) (2020) 105704.

[17] K. Ahmed, T. Akbar, T. Muhammad, M. Alghamdi, Heat transfer characteristics of MHD flow of Williamson nanofluid over an exponential permeable stretching curved surface with variable thermal conductivity, *Case Studies in Thermal Engineering*, 28 (2021) 101544.

[18] M. Jawad, A. Saeed, T. Gul, A. Khan, The magnetohydrodynamic flow of a nanofluid over a curved exponentially stretching surface, *Heat Transfer-Asian Res*. 50 (2021) 5356- 5379.

[19] M. Naveed, Z. Abbas, M. Sajid, Hydromagnetic flow over an unsteady curved stretching surface, *Engineering Science and Technology, an International Journal* 19 (2016) 841–845.

[20] Mishra, A, Pandey, AK, Kumar, M. Thermal performance of Ag–water nanofluid flow over a curved surface due to chemical reaction using Buongiorno's model. *Heat Transfer*. 2021; 50: 257– 278. https://doi.org/10.1002/htj.21875

[21] W. Ibrahim and G. Kuma, Magnetohydrodynamic flow of nanofluid due to non-linearly curved stretching surface with high order slip flow, *Heat Transfer-Asian Res*. 48 (2019) 3724- 3748.

[22] T. Hayat, M. Rashid, M. Imtiaz, A. Alsaedi, MHD convective flow due to a curved surface with thermal radiation and chemical reaction. *J Mol. Liq*. 225 (2017) 482–489.

[23] Alok Kumar Pandey, Manoj Kumar, Natural convection and thermal radiation influence on nanofluid flow over a stretching cylinder in a porous medium with viscous dissipation, *Alexandria Engineering Journal*, Volume 56, Issue 1,2017,Pages 55-62.

[24] Pandey, AK, Upreti, H. Mixed convective flow of Ag–H_2O magnetic nanofluid over a curved surface with volumetric heat generation and temperature dependent viscosity. *Heat Transfer*. 2021; 50: 7251- 7270. https://doi.org/10.1002/htj.22227

[25] M. Riaz, M. I. Khan, N. B. Khan, M. Jameel, Magnetohydrodynamics (MHD) radiated nanomaterial viscous material flow by a curved surface with second order slip and entropy generation, *Computer Methods and Programs in Biomedicine* 189 (2020) 105294.

[26] Bhatti, M.M., Bég, O.A., Ellahi, R., Abbas T., Natural convection non-Newtonian emhd dissipative flow through a microchannel containing a non-Darcy porous medium: homotopy perturbation method study. *Qual. Theory Dyn. Syst.* **21**, 97 (2022).

[27] V.K. Naga N, Ishikawa G, Noguchi K, Takahashi K, Watanabe K, Yamato M. Magnetic-field-induced alignment of low molecular weight polyethylene. *Polymer.* 2013; 54:784-790.

[28] A. Shahid, M. M. Bhatti, O. Anwar Bég and A. Kadir, Numerical study of radiative Maxwell viscoelastic magnetized flow from a stretching permeable sheet with the Cattaneo–Christov heat flux model, *Neural Computing and Applications,* 30, 3467–3478 (2018).

[29] M. Naveed, Z. Abbas, M. Sajid, MHD flow of a micropolar fluid due to a curved stretching sheet with thermal radiation, *J. Appl. Fluid Mech*. 9 (1) (2016) 131–138.

[30] Ankita Bisht and O. Anwar Bég, Computation of thermo-magneto-bioconvection in Sisko nanofluid flow over a curved stretching sheet doped with gyrotactic microorganisms, *ASME J. Heat Transfer, communicated (2022).*

[31] M. Gnaneswara Reddy, M.S. Rani, M.M. Praveen, K.G. Kumar, Comparative study of different non-Newtonian fluid over an elaborated sheet in the view of dual stratified flow and Ohmic heat, *Chemical Physics Letters* 784, (2021) 139096.

[32] T. Shabbir, M. Mushtaq, M.I. Khan, T. Hayat, Modeling and numerical simulation of micropolar fluid over a curved surface: Keller box method, *Comput. Methods Progr. Biomed.* 187 (2020) 105220.

[33] S.Maity and P. K. Kundu, Magnetically driven chemically reactive Casson nanofluid flow over curved surface with thermal radiation, *Heat Transfer-Asian Res.*, 51(6) (2022), 4882-4905.

[34] Bhatti MM, Sait SM, Ellahi R. Magnetic nanoparticles for drug delivery through tapered stenosed artery with blood based non-Newtonian fluid. *Pharmaceuticals*. 2022; 15(11):1352. https://doi.org/10.3390/ph15111352.

[35] Xiao-Hong Zhang, Awatef Abidi, A. El-Sayed Ahmed, M. Riaz Khan, M. A. El-Shorbagy, Meshal Shutaywi , Alibek Issakhov, Ahmed M. Galal, MHD stagnation point flow of nanofluid over a curved stretching/ shrinking surface subject to the influence of Joule heating and convective condition, *Case Studies in Thermal Engineering* 26 (2021) 101184.

[36] T. Hayat, S. Qayyum, M. Imtiaz, A. Alsaedi, Double stratification in flow by curved stretching sheet with thermal radiation and Joule heating, *ASME.* J. Thermal Sci. Eng. Appl. 10(2) (2018) 021010.

[37] K. Ananth Kumar, V. Sugunamma, N. Sandeep, Effect of thermal radiation on MHD Casson fluid flow over an exponentially stretching curved sheet, *J. Thermal Analysis Calorim.* 140 (2020) 2377–2385.

[38] M. Ferdows, M. Murtaza, M. Bangalee, M.S. Hossain, Effects of mixed convection and radiation parameter on MHD heat transfer flow over a curved stretching sheet, *Dhaka University J. Sci*. 69(3) (2022) 171–178.

[39] V. Sridhar, K. Ramesh, D.Tripathi, Vivekanand, Analysis of thermal radiation, Joule heating, and viscous dissipation effects on blood-gold couple stress nanofluid flow driven by electroosmosis, *Heat Transfer-Asian Res*. 2022; 51 (5): 4080-4101.

[40] M. Sajid, S. A. Iqbal, M. Naveed, Z. Abbas, Joule heating and magnetohydrodynamic effects on ferrofluid (Fe3O4) flow in a semi-porous curved channel, *Journal of Molecular Liquids* 222 (2016) 1115–1120.

[41] M.D. Shamshuddin, S.R. Mishra, O. Anwar Bég and A. Kadir, Unsteady reactive magnetic radiative micropolar flow, heat and mass transfer from an inclined plate with Joule heating: a *model for magnetic polymer processing, Proc. IMechE- Part C. – Mechanical Engineering Science,* 223, 4, 1-8 (2019).

[42] M. Shamshuddin, U. S. Khan, O. Anwar Bég, T.A. Bég, Hall current, viscous and Joule heating effects on steady radiative 3-D magneto-power-law polymer dynamics from an exponentially stretching sheet with power-law slip velocity: a numerical study, *Thermal Science and Engineering Progress, 20 (2020) 100732. doi.org/10.1016/j.tsep.2020.100732 (13 pages)*

[43] J. Prakash, D. Tripathi, N. Akkurt, O Anwar Bég, Tangent hyperbolic non-Newtonian radiative bioconvection nanofluid flow from a bi-directional stretching surface with electro-magneto-hydrodynamic, Joule heating and modified diffusion effects. *Eur. Phys. J. Plus*, 137, 472 (2022).

[44] S. A. Gaffar, V. R. Prasad, B. Vijaya and O. Anwar Bég, Mixed convection flow of magnetic viscoelastic polymer from a non-isothermal wedge with Biot number effects, *Int. J. Engineering Mathematics*, Volume 2015, Article ID 287623, 15 pages (2015).

[45] P. Rana, R. Bhargava, O. Anwar Bég and A. Kadir, Finite element analysis of viscoelastic nanofluid flow with energy dissipation and internal heat source/sink effects, *Int. J. Applied Computational Mathematics* 3 (2) 1421–1447 (2017).

[46] Kashevskii BE, Kordonskii VI, Prokhorov IV, Demchuk SA, Gorodkin SR. Relaxation of viscous stresses in magnetorheological suspension. *Magnetohydrodynamics (Russia)*. 1990; 26:140-143.

[47] Kimura T. Study on the effect of magnetic field on polymeric materials and its application. *Polymer Journal*. 2003; 35:823-843.

[48] Mantripragada S, Wang X, Gordaninejad F, Hu B, Fuchs A. Rheological properties of novel magnetorheological fluids. *International Journal of Modern Physics B*. 2007; 21:4849-4857.